



Increase of the oxygen vacancy component in bridgmanite with temperature

HPSTAR
896-2019



Zhaodong Liu^{a,*}, Masaki Akaogi^b, Tomoo Katsura^{a,c}

^a Bayerisches Geoinstitut, University of Bayreuth, 95440 Bayreuth, Germany

^b Department of Chemistry, Gakushuin University, 171-8588 Tokyo, Japan

^c Center for High Pressure Science & Technology Advanced Research, Beijing, 100094, China

ARTICLE INFO

Article history:

Received 21 May 2018

Received in revised form 5 October 2018

Accepted 12 October 2018

Available online 29 October 2018

Editor: J. Brodholt

Keywords:

oxygen vacancy

bridgmanite

temperature

velocity

volatile

slab stagnation

ABSTRACT

The oxygen vacancy (OV, MgAlO_{2.5}) contents in bridgmanite with periclase and/or a calcium ferrite-type MgAl₂O₄–Mg₂SiO₄ phase (CF-phase) were investigated at temperatures of 1700, 2000, and 2400 K and a pressure of 27 GPa using an ultrahigh-pressure multi-anvil press. The OV content increases significantly with increasing temperature by consuming coexisting periclase and the charge-coupled (CC, AlAlO₃) component in bridgmanite. The increase in OV component at high temperature is promoted by its high entropy. The CC components increase largely with temperature compared with the OV content in bridgmanite coexisting with CF-phase and periclase because the partition coefficient of Mg and Al between bridgmanite and CF-phase approaches unity because of the mixing entropy. The partial molar volumes of OV and CC bridgmanite endmembers at ambient conditions were constrained to be 26.64 and 25.79 cm³/mol, respectively, with densities of 3.428 and 3.955 g/cm³. By assuming linear relationships between wave velocities and density, the OV component may therefore cause a velocity reduction by one order of magnitude larger than the CC component at constant Al content in bridgmanite. The concomitant increase and decrease in OV and CC contents with temperature enhance V_p and V_s reductions by 0.7% and 2.5% in addition to anharmonic effects. The OV component in bridgmanite in subducted slabs is zero because of low temperature, and the transport of water and argon trapped by the OV component into the lower mantle by bridgmanite is therefore not expected. The storage capacity of these volatiles in subducted slabs will thus be significantly lower than the warm ambient mantle. Since the OV component is expected to enhance diffusion creep, the present results may explain slab stagnation in the mid-mantle due to low OV contents at low temperature, and vertically straight plumes in the lower mantle due to high OV contents at high temperature.

© 2018 Elsevier B.V. All rights reserved.

1. Introduction

Bridgmanite is the major host phase of aluminum (Al) in the Earth's lower mantle (Irifune, 1994). The incorporation of Al can produce significant effects on the chemical and physical properties of bridgmanite, including iron oxidation (McCammon, 1997; Frost et al., 2004), Fe–Mg partitioning (Frost and Langenhorst, 2002), elasticity (e.g., Zhang and Weidner, 1999; Brodholt, 2000; Jackson et al., 2004; Walter et al., 2004, 2006), and electrical conductivity (e.g., Xu et al., 1998; Yoshino et al., 2016). Al is incorporated into bridgmanite via formation of both charge-coupled (CC) and oxygen vacancy (OV) components in the forms of AlAlO₃ and MgAlO_{2.5}, respectively (Hirsch and Shankland, 1991). In the CC

component, Al³⁺ ions occupy Mg²⁺ and Si⁴⁺ sites (A- and B-sites hereafter) in the orthorhombic perovskite structure, whereas they occupy only B-sites and create oxygen vacancies in the OV component. Bridgmanite containing an OV component is thought to be more compressible than that with a CC component, suggesting that the shallower part of the lower mantle may be significantly weaker than deeper regions (Brodholt, 2000). The OV component has also been suggested to reduce the creep strength of bridgmanite, which may account for the viscosity increase in the mid-mantle (Liu et al., 2017a). In addition, the presence of an OV component in bridgmanite may induce volatiles such as water (Navrotsky, 1999) and noble gases (Shcheka and Keppler, 2012) into the lower mantle. Hence, it is important to evaluate the OV contents in bridgmanite at relevant conditions for better understanding the physical and chemical properties of the Earth's lower mantle.

Previous high-pressure and high-temperature synthesis experiments (Navrotsky et al., 2003; Kojitani et al., 2007a) suggested

* Corresponding author.

E-mail address: zhaodong.liu@uni-bayreuth.de (Z. Liu).

that significant amounts of OV component may be present in aluminous bridgmanite at 27 GPa and 1873 K in MgO-saturated MgSiO_3 – $\text{MgAlO}_{2.5}$ systems. These results were confirmed by ^{27}Al nuclear magnetic resonance spectroscopy (Stebbins et al., 2003), which indicated that Al preferentially substitutes for Si^{4+} in the B-sites. More recently, Liu et al. (2017a) found that bridgmanite synthesized from a glass starting composition of $\text{En}_{90}\text{Brm}_{10}$ (En: MgSiO_3 enstatite; Brm: $\text{MgAlO}_{2.5}$ brownmillerite) at 27 GPa and 2000 K contains 5.7 mol% OV component. This concentration is significantly higher than values of 2.5–4.5 mol% synthesized at a lower temperature of 1873 K and identical pressure reported by Navrotsky et al. (2003) and Kojitani et al. (2007a), suggesting that temperature may affect the OV content in bridgmanite. A temperature effect was also observed by Andraut et al. (2007) based on a compression study of aluminous bridgmanite using a laser-heated diamond anvil cell (LHDAC): the bulk modulus of bridgmanite synthesized at 1800 K (272 GPa) is significantly higher than that at 2300 K (244 GPa). Because bulk modulus is believed to decrease with increasing OV content (Brodholt, 2000), the lower bulk modulus of bridgmanite synthesized at higher temperature should imply a positive correlation between the synthesis temperature and OV content. However, Andraut et al. (2007) were not able to determine OV content owing to very small sample sizes in the LHDAC. Temperature is the most essential parameter for mantle dynamics because it differs significantly between cold subducted slabs (~1000–1400 K) and ambient lower mantle (~2000–2300 K) (e.g., Brown and Shankland, 1981; Kirby et al., 1996; Eberle et al., 2002). Nevertheless, the effect of temperature on the maximum OV content in bridgmanite remains unclear. Furthermore, it is important to note that both theoretical (Brodholt, 2000) and experimental studies (Walter et al., 2006; Andraut et al., 2007) has reported that the proportion of the OV component may decrease rapidly at pressures above 24–25 GPa, which was recently confirmed by Liu et al. (2017a). Thus, the pressure effect has already been established.

In the present study, we determined the maximum OV contents along with the CC content in bridgmanite both with and without MgO-rich phases in the MgSiO_3 – $\text{MgAlO}_{2.5}$ and MgSiO_3 – Al_2O_3 systems at temperatures of 1700, 2000, and 2400 K and a constant pressure of 27 GPa using a multi-anvil press with tungsten carbide anvils. The results presented here are used to discuss the complicated chemistry and elasticity of bridgmanite and the volatile storage capacity of the lower mantle.

2. Experimental methods

Five starting materials were prepared in the present study. Two glass starting compositions were $\text{En}_{90}\text{Brm}_{10}$ (the subscripted number represents mol%; En: MgSiO_3 enstatite; Brm: $\text{MgAlO}_{2.5}$ brownmillerite) and $\text{En}_{95}\text{Cor}_5$ (Cor: Al_2O_3 corundum), which potentially form a single bridgmanite phase with either of the OV and CC components, respectively, as the principle component. Glasses were prepared from oxide mixtures of reagent grade MgO, SiO_2 , and Al_2O_3 , fused at 2000 K for 30 min and quenched into ice water. We repeated this process three times to fabricate homogeneous glasses. We also prepared powdered mixtures composed of 70 wt.% orthopyroxene with either an $\text{En}_{95}\text{Cor}_5$ or $\text{En}_{90}\text{Brm}_{10}$ composition (synthesized at 3 GPa and 1400 K for 5 h) with 30 wt.% MgO, to examine reaction equilibration of run products by synthesizing bridgmanite obtained via different synthetic routes. It is important to note that the resulting bridgmanite should coexist with periclase and be saturated with MgO in the case of these two starting materials. A fine-grained oxide mixture with an $\text{En}_{70}\text{Brm}_{30}$ composition was also prepared, so that bridgmanite coexists with another Al_2O_3 -rich phase in addition to periclase.

Table 1
Experimental conditions and run products.

Run No.	Start comp.	$P/T/t$ (GPa)/(K)/(h)	Phases
IRIS506	$\text{En}_{90}\text{Brm}_{10}$	27/1700/30	Brg
	$\text{En}_{70}\text{Brm}_{30}$	–	Brg + CF + Per
	$\text{En}_{95}\text{Cor}_5$	–	Brg
IRIS420	$\text{En}_{90}\text{Brm}_{10}$	27/2000/20	Brg
	$\text{En}_{90}\text{Brm}_{10}$ + MgO	–	Brg + Per
	$\text{En}_{70}\text{Brm}_{30}$	–	Brg + CF + Per
IRIS512	$\text{En}_{90}\text{Brm}_{10}$	27/2400/4	Brg
	$\text{En}_{90}\text{Brm}_{10}$ + MgO	–	Brg + Per
	$\text{En}_{70}\text{Brm}_{30}$	–	Brg + CF + Per
IRIS527	$\text{En}_{95}\text{Cor}_5$	27/2400/6	Brg
	$\text{En}_{95}\text{Cor}_5$ + MgO	–	Brg + Per

–: the same as the above conditions.

Abbreviations: Brg, bridgmanite; CF: calcium ferrite-type structure of MgAl_2O_4 ; Per, periclase.

The starting materials were loaded into a platinum (Pt) capsule, and heated to 800 K for 1 h to minimize water content before welding. High-pressure and high-temperature experiments were conducted at temperatures of 1700, 2000, and 2400 K under a constant pressure of 27 GPa for 4 to 30 h using a Cr_2O_3 -doped MgO octahedron with an edge length of 7 mm and hard TF05 tungsten carbide anvils with a truncated edge length of 3 mm with a press load of 15 MN in a Kawai-type multi-anvil apparatus (IRIS-15) at the Bayerisches Geoinstitut, University of Bayreuth (Ishii et al., 2016). The cell assembly included a LaCrO_3 sleeve heater and MgO sleeve for accommodating the Pt capsule. Temperature was measured using a W_{97}Re_3 – $\text{W}_{75}\text{Re}_{25}$ thermocouple positioned at the center of the heater and adjacent to the base of the Pt capsule. No pressure correction was applied to thermocouple emf. Experimental pressures at high temperature were calibrated based on the solubility of Al_2O_3 in bridgmanite in equilibrium with corundum (Liu et al., 2016, 2017b).

Recovered samples were mounted in epoxy resin, ground to expose the central portion, and then polished using 0.25 μm diamond paste. Textural observations and chemical analyses of the recovered samples were performed using a LEO1530 scanning electron microscope (SEM) and JEOL JXA-8200 electron probe microanalyzer (EPMA) operating at an acceleration voltage of 15 kV and beam current of 5 nA with enstatite and forsterite as standards for Mg and Si, respectively, and corundum as a standard for Al. We also determined the composition of pure MgSiO_3 bridgmanite using the same settings as a benchmark analysis, and obtained an accurate Mg/Si ratio of 1.008 ± 0.005 . Samples were extracted from the Pt capsules after compositional analysis. XRD profiles were collected over a span of approximately two hours. Phases in the samples were identified using a micro-focused X-ray diffractometer with a Co anode operated at an acceleration voltage of 40 kV and beam current of 500 μA . The MgSiO_3 bridgmanite was used as an external standard to calibrate the Bragg angle (2θ) of the instrument.

3. Results

Experimental conditions and run products are summarized in Table 1.

3.1. Phase assemblages

Fig. 1 shows the XRD patterns of all run products. These results show that the $\text{En}_{90}\text{Brm}_{10}$ and $\text{En}_{95}\text{Cor}_5$ starting glasses crystallized into a single bridgmanite phase. The mixtures of $\text{En}_{90}\text{Brm}_{10}$ plus MgO and $\text{En}_{95}\text{Cor}_5$ plus MgO crystallized into a phase assemblage of bridgmanite plus periclase. The $\text{En}_{70}\text{Brm}_{30}$ sample crystallized

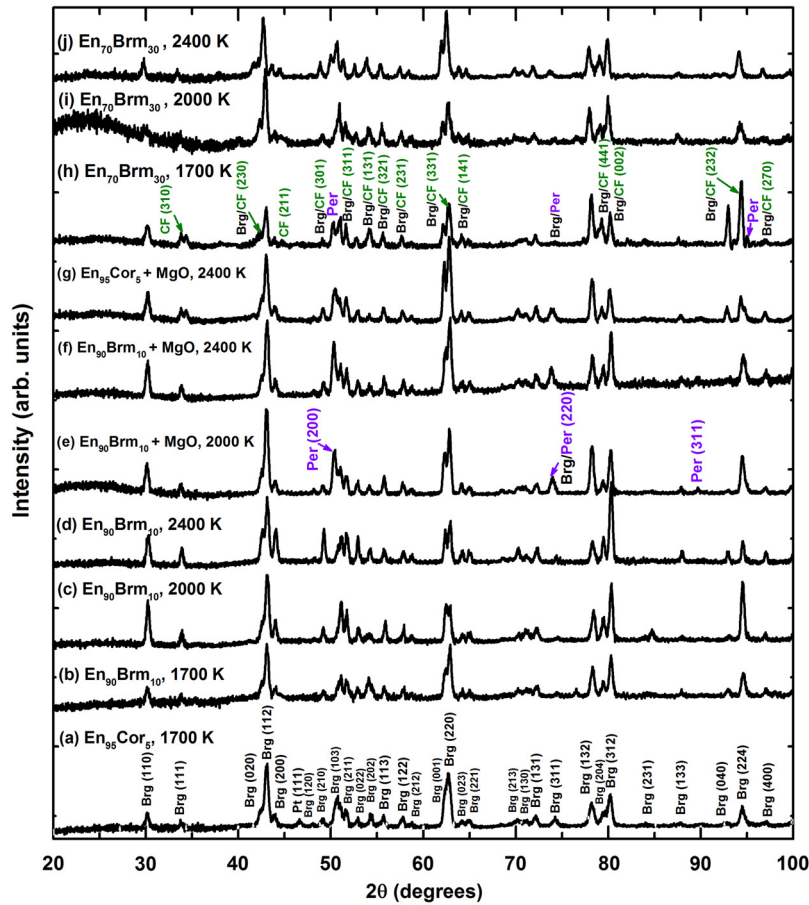


Fig. 1. XRD patterns of run products at 1700, 2000, and 2400 K at a pressure of 27 GPa. The number in parentheses represents miller indices of the first appearing phase. Abbreviations: Brg, bridgmanite; CF: calcium ferrite-type structure of MgAl_2O_4 ; Per, periclase.

into bridgmanite, periclase, and a CF-phase (calcium ferrite-type structure of MgAl_2O_4 – Mg_2SiO_4). Fig. 2 shows back-scattered electron (BSE) images of the corresponding products. In these images, bridgmanite appears as gray grains, typically 3–10 μm in dimension, and some micro-cracks occur on the surfaces. On the other hand, periclase appears as dark gray grains, and the CF-phase shows smooth outlines. Some amorphization occurs in some bridgmanite grains in the samples of Figs. 2a, 2b, and 2c as shown by a relatively bright color compared with gray bridgmanite grains, which may be caused by exposure under the electron beam during SEM analysis. Nevertheless, grain boundaries of each phase were clearly visible in the run products.

3.2. Phase compositions

The compositions of bridgmanite and coexisting phases are listed in Table 2. We confirmed that all phases are fairly uniform in composition. In addition, the bridgmanite from $\text{En}_{90}\text{Brm}_{10}$ shows similar compositions with those from the mixture of $\text{En}_{90}\text{Brm}_{10}$ plus MgO, and the BSE images show that all phases have relatively clear grain boundaries. These observations suggest that chemical equilibrium was achieved in the experiments.

Fig. 3a presents variations of the OV and CC contents with temperature obtained using different starting compositions. The OV and CC contents were calculated from the following equation: $\text{Mg}_x\text{Al}_z\text{Si}_y\text{O}_{x+1.5z+2y} = y\text{MgSiO}_3 + (x-y)\text{MgAlO}_{2.5}$ (OV) + $(z-x+y)/2\text{AlAlO}_3$ (CC), and $x+y+z=2$ (Liu et al., 2017a). In the case of the single bridgmanite made from $\text{En}_{90}\text{Brm}_{10}$, the OV content increases from 3.0 ± 0.8 mol% at 1700 K to 5.2 ± 0.7 mol% at

2000 K to 6.2 ± 0.9 mol% at 2400 K. In contrast, the CC content concomitantly decreases from 3.5 ± 0.4 mol% at 1700 K to 1.7 ± 0.5 mol% at 2400 K. For the mixture of $\text{En}_{90}\text{Brm}_{10}$ plus MgO, bridgmanite coexisting with periclase possesses essentially the same OV and CC contents as those without periclase within the analytical uncertainties. It is noted that periclase coexisting with bridgmanite contains small amounts of Al_2O_3 ranging from 0.79 ± 0.03 wt.% at 2000 K to 1.20 ± 0.07 wt.% at 2400 K (Table 2). The inverse correlation between the OV and CC contents is a result of the constant total Al content in bridgmanite within the samples.

As expected, the OV contents in bridgmanite from both the $\text{En}_{90}\text{Brm}_{10}$ glass and $\text{En}_{90}\text{Brm}_{10}$ plus MgO are significantly higher than those in the samples obtained from the $\text{En}_{95}\text{Cor}_5$ glass at all temperatures (Table 2). The OV content synthesized from $\text{En}_{95}\text{Cor}_5$ plus MgO is 4.5 ± 1.0 mol% at 2400 K. This value is significantly higher than 1.0 ± 0.6 mol% obtained from $\text{En}_{95}\text{Cor}_5$ but lower than that of 6.2 ± 0.9 mol% obtained from $\text{En}_{90}\text{Brm}_{10}$ at the same temperature, again within the analytical uncertainties.

The OV and CC contents in bridgmanite coexisting with CF-phase and periclase from $\text{En}_{70}\text{Brm}_{30}$ increase from 2.9 ± 0.7 and 4.6 ± 0.6 mol% at 1700 K to 4.3 ± 0.9 and 7.3 ± 0.8 mol% at 2400 K, respectively (Fig. 3b). This increase of the CC component with temperature is different from the case without a CF-phase (Fig. 3a). In contrast, the Al content in the CF-phase decreases with increasing temperature: the MgAl_2O_4 contents in the CF-phase are 76 ± 2 , 64 ± 1 , and 61 ± 1 mol% at 1700, 2000, and 2400 K, respectively (Table 2). The Al partitioning in these phases will be discussed in detail later.

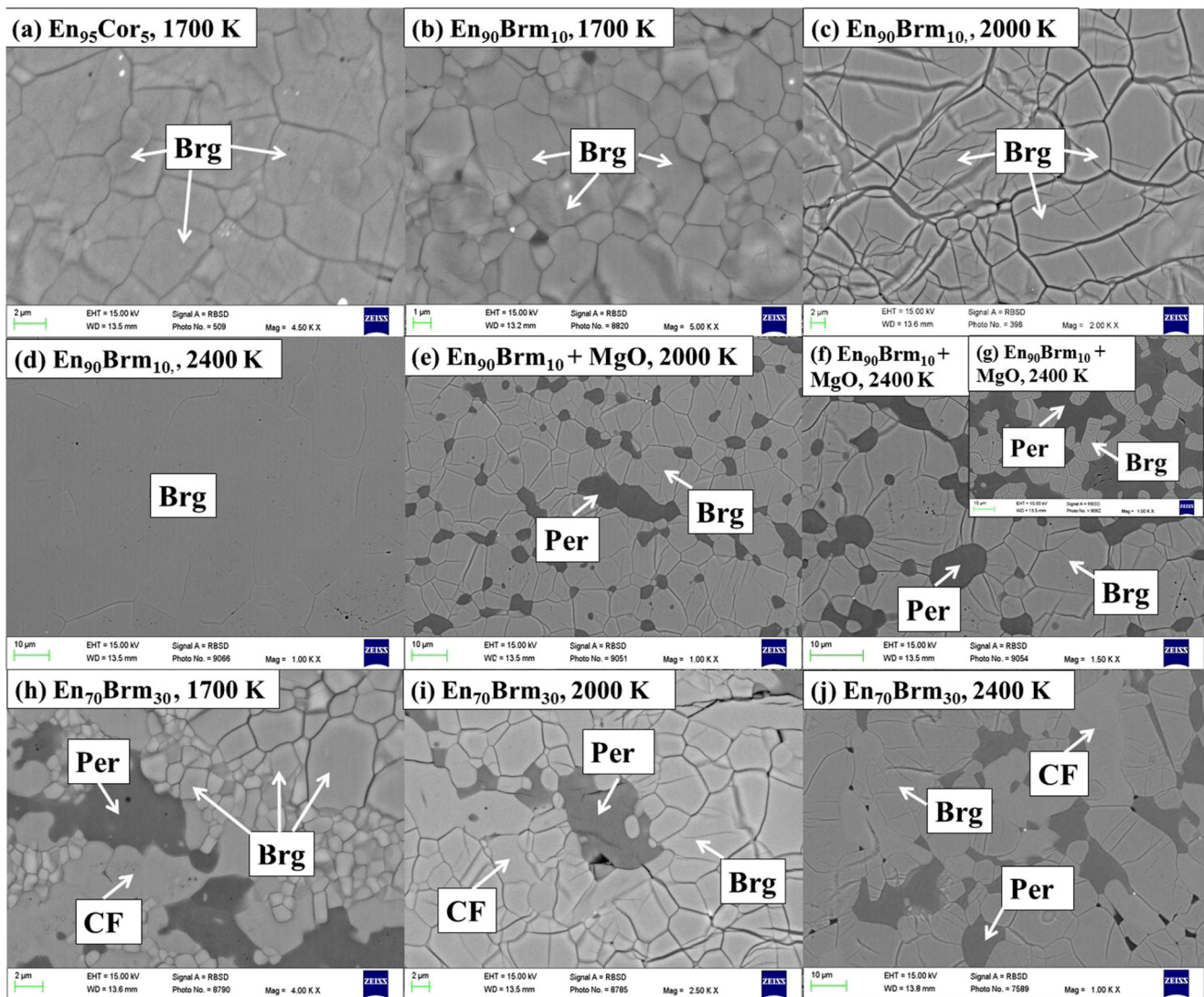


Fig. 2. BSE images of run products at 1700, 2000, and 2400 K under a pressure of 27 GPa. Abbreviations: Brg, bridgmanite; CF: calcium ferrite-type structure of MgAl_2O_4 ; Per, periclaise.

3.3. Molar volume of OV- and CC-dominated bridgmanite

The molar volumes of the synthetic bridgmanite are listed in Table S1 in the Supplementary material. Fig. 4a shows the molar volumes of bridgmanite with an Al pfu (pfu: per formula units based on the total cation number of 2) of 0.1 against synthesis temperature. As mentioned above, the OV component dominates in the $\text{En}_{90}\text{Brm}_{10}$ samples with and without MgO, whereas the CC component dominates in the $\text{En}_{95}\text{Cor}_5$ samples, and are called the OV- and CC-dominated bridgmanite, respectively. The molar volume of the OV-dominated bridgmanite increases from $24.51 \pm 0.05 \text{ cm}^3/\text{mol}$ at 1700 K to $24.55 \pm 0.05 \text{ cm}^3/\text{mol}$ at 2000 K to $24.60 \pm 0.05 \text{ cm}^3/\text{mol}$ at 2400 K. The CC-dominated bridgmanite has a molar volume of 24.48 ± 0.06 and $24.51 \pm 0.05 \text{ cm}^3/\text{mol}$ at 1700 and 2400 K, respectively, and is thus insensitive to synthesis temperature. The increase of molar volume of the OV-dominated bridgmanite with temperature is supported by Brodholt (2000).

Fig. 4b shows the molar volumes of bridgmanite against the OV and CC content in our present and recent studies (Liu et al., 2017b). To distinguish the effect of the OV component on the molar volume, we first fitted the volumes of the CC-bearing but OV-absent bridgmanite to a linear function, and obtained $V(X) = 24.44 + (dV/dX) \times X$, where V is the molar volume in cm^3/mol , and X is the CC content in mol%. Thus, the CC component increases

the molar volume of bridgmanite at a rate of $0.0135 (4) \text{ cm}^3/\text{mol}$ (The number in parentheses represents the standard deviation of the last digit). From these values, the molar volume and density of the hypothetical CC endmember are found to be $25.79 (5) \text{ cm}^3/\text{mol}$ and $3.955 (8) \text{ g/cm}^3$, which are almost consistent with those estimated by Akaogi and Ito (1999). These two values are 5.5 (2)% larger and $-3.7 (2)\%$ smaller than pure MgSiO_3 bridgmanite, respectively ($24.44 \text{ cm}^3/\text{mol}$ and 4.108 g/cm^3 , Horiuchi et al., 1987). We subtracted the effect of the CC component from the OV-dominated bridgmanite to obtain the molar volume of the pure OV-dominated bridgmanite. By fitting, we obtained the following equation: $V(X) = 24.44 + 0.022(1) \times X$. Thus, the OV component increases the molar volume of bridgmanite at a rate of $0.022 (1) \text{ cm}^3/\text{mol}$, which is larger by 6% than that of CC component. From these values, the molar volume and density of the hypothetical OV endmember are found to be $26.64 (10) \text{ cm}^3/\text{mol}$ and $3.428 (13) \text{ g/cm}^3$, which are 9.0 (4)% larger and $-16.2 (4)\%$ smaller than pure MgSiO_3 bridgmanite. It is emphasized that the density of the OV component is particularly small, which is partly because of its larger molar volume but more importantly because of its smaller formula weight due to the oxygen vacancy. The molar weights of MgSiO_3 , Al_2O_3 and $\text{MgAlO}_{2.5}$ are 100.39, 101.96 and 91.28 g/mol, respectively.

Table 2

The compositions of the run products. Oxide analyses are reported in wt.%. The total number of cations for bridgmanite, CF-phase, and periclase is normalized to two, three, and one, respectively. Number in parentheses represents standard deviations for the last digit (s).

Start comp.	Phases	MgO	Al ₂ O ₃	SiO ₂	Total	Mg	Al	Si	O	Brg			CF	
										OV (mol%)	CC (mol%)	En (mol%)	Mg(MgSi)O ₄ (mol%)	MgAl ₂ O ₄ (mol%)
IRIS506 (1700 K)														
En ₉₅ Cor ₅	Brg [n = 35]	38.68 (56)	5.01 (13)	57.71 (48)	101.39 (86)	0.951 (7)	0.097 (2)	0.952 (7)	3.000 (7)	−0.1 (14)	4.9 (7)	95.2 (7)		
En ₇₀ Brm ₃₀	Brg [n = 28]	39.05 (46)	6.27 (55)	56.46 (70)	99.17 (59)	0.954 (6)	0.121 (11)	0.925 (7)	2.986 (3)	2.9 (7)	4.6 (6)	92.5 (7)		
	CF [n = 8]	35.14 (77)	53.29 (97)	10.24 (59)	98.67 (65)	1.253 (17)	1.502 (28)	0.245 (14)	3.996 (7)				24 (1)	76 (2)
	Per [n = 5]	99.44 (56)	0.22 (2)		99.67 (67)	0.998 (0)	0.002 (0)		1.001 (0)					
En ₉₀ Brm ₁₀	Brg [n = 55]	39.46 (30)	5.14 (15)	56.99 (64)	101.59 (70)	0.965 (4)	0.099 (3)	0.935 (4)	2.985 (4)	3.0 (8)	3.5 (4)	93.5 (4)		
IRIS420 (2000 K)														
En ₉₀ Brm ₁₀	Brg [n = 20]	39.38 (31)	5.12 (18)	55.55 (36)	100.05 (52)	0.976 (4)	0.100 (3)	0.924 (4)	2.974 (4)	5.2 (7)	2.4 (4)	92.4 (4)		
En ₇₀ Brm ₃₀	Brg [n = 30]	38.08 (28)	8.31 (38)	54.76 (47)	101.15 (72)	0.936 (4)	0.161 (7)	0.903 (5)	2.983 (5)	3.3 (5)	6.4 (4)	90.3 (6)		
	CF [n = 10]	37.40 (35)	46.26 (73)	14.78 (50)	98.43 (50)	1.338 (12)	1.308 (19)	0.355 (12)	4.009 (6)				36 (1)	64 (1)
	Per [n = 5]	99.37 (69)	0.81 (6)		100.81 (67)	0.994 (1)	0.006 (0)		1.003 (0)					
En ₉₀ Brm ₁₀ + MgO	Brg [n = 26]	40.45 (32)	4.99 (9)	56.87 (37)	102.31 (70)	0.980 (6)	0.096 (2)	0.924 (6)	2.972 (6)	5.6 (12)	2.0 (6)	92.4 (6)		
	Per [n = 5]	99.91 (16)	0.79 (3)	0.05 (1)	100.75 (14)	0.993 (0)	0.006 (1)		1.003 (0)					
IRIS512 (2400 K)														
En ₇₀ Brm ₃₀	Brg [n = 40]	37.30 (32)	9.66 (67)	53.03 (68)	100.03 (98)	0.927 (8)	0.190 (13)	0.884 (7)	2.979 (5)	4.3 (9)	7.3 (8)	88.4 (8)		
	CF [n = 10]	38.84 (77)	43.86 (56)	16.17 (51)	98.87 (104)	1.381 (16)	1.233 (22)	0.386 (9)	4.002 (6)				39 (1)	61 (1)
	Per [n = 5]	98.18 (56)	1.30 (5)	0.03 (1)	99.51 (62)	0.990 (0)	0.010 (0)		1.005 (0)					
En ₉₀ Brm ₁₀	Brg [n = 40]	40.19 (39)	5.02 (13)	56.11 (61)	101.31 (85)	0.983 (5)	0.097 (3)	0.920 (5)	2.969 (5)	6.2 (9)	1.7 (5)	92.0 (5)		
En ₉₀ Brm ₁₀ + MgO	Brg [n = 26]	40.09 (32)	4.98 (14)	55.89 (57)	100.95 (62)	0.984 (6)	0.097 (3)	0.920 (5)	2.968 (5)	6.4 (9)	1.6 (5)	92.0 (5)		
	Per [n = 5]	98.23 (41)	1.20 (7)	0.05 (1)	99.47 (39)	0.991 (1)	0.009 (1)		1.005 (0)					
IRIS527 (2400 K)														
En ₉₅ Cor ₅ + MgO	Brg [n = 25]	40.15 (47)	4.89 (35)	57.09 (42)	102.13 (69)	0.975 (5)	0.094 (7)	0.931 (7)	2.978 (5)	4.5 (10)	2.5 (5)	93.0 (7)		
	Per [n = 4]	98.30 (49)	1.14 (11)	0.34 (30)	99.78 (19)	0.989 (2)	0.009 (0)	0.002 (2)	1.007 (2)					
En ₉₅ Cor ₅	Brg [n = 10]	39.19 (38)	5.06 (12)	57.83 (47)	102.07 (76)	0.956 (3)	0.098 (3)	0.946 (3)	2.995 (3)	1.0 (6)	4.4 (3)	94.6 (3)		

Abbreviations: Brg, bridgmanite; CF: calcium ferrite-type structure of MgAl₂O₄; Per, periclase; OV: MgAlO_{2.5}; CC: AlAlO₃; En: MgSiO₃.
n is the number of analyses.

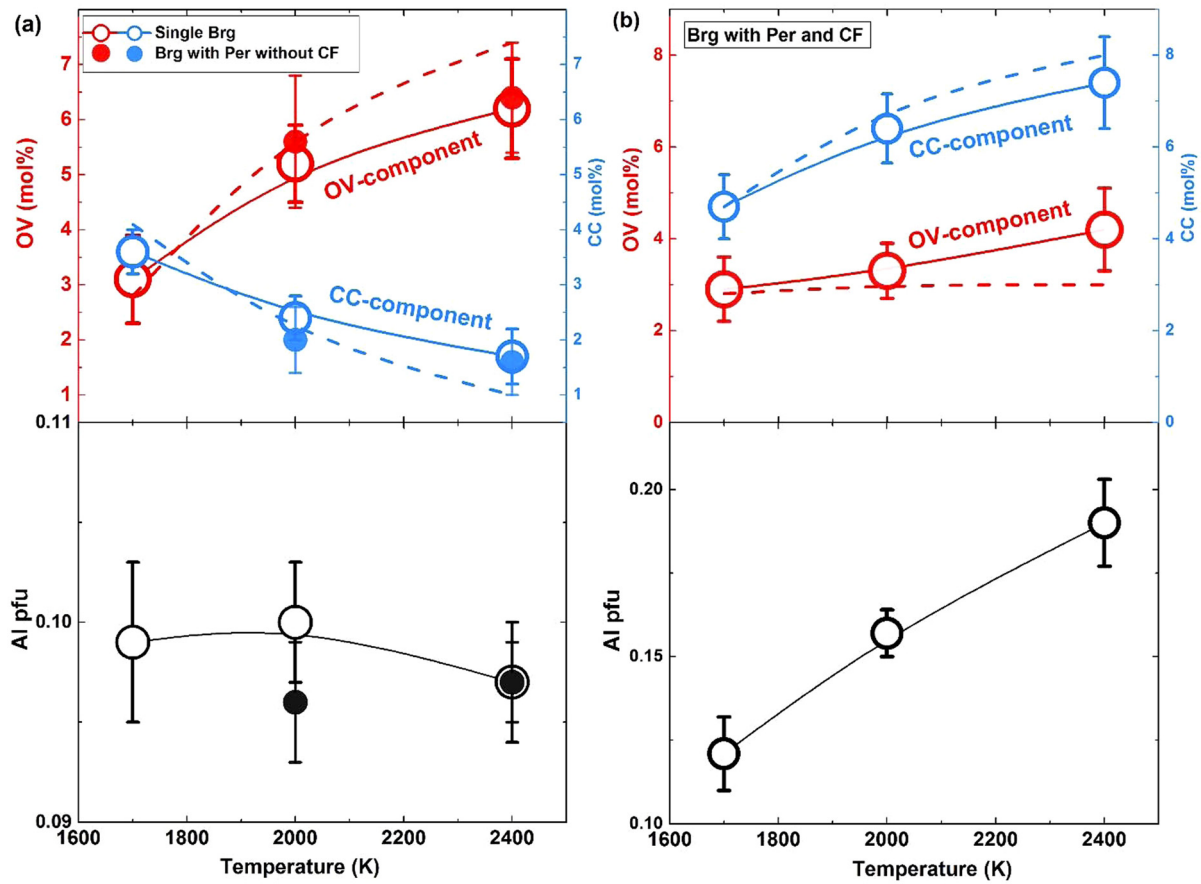


Fig. 3. The content of OV and CC component (upper) and Al pfu (per formula units) (bottom) with temperature for (a) single-phase bridgmanite for En₉₀Brm₁₀ (open symbols) and that coexisting with periclase for mixture of En₉₀Brm₁₀ and MgO (solid symbols) and (b) bridgmanite coexisting with periclase and CF phase for En₇₀Brm₃₀. Solid lines are the tendency of the experimental data with temperature, while dashed lines are thermodynamic results through a minimum of Gibbs free energy of reaction (1) by $\Delta G_{R1}(P, T, X) = \Delta H_T^0 - T\Delta S_T^0 + \int_1^P \Delta V_{P,T} + RT \ln \frac{(X_{MgAlO_{2.5}}^{Brg})^2}{(X_{MgO}^{Per})^2 X_{AlAlO_3}^{Brg}} - W_{AlAlO_3}^{Brg} (1 - X_{AlAlO_3}^{Brg})^2 + 2W_{MgAlO_{2.5}}^{Brg} (1 - X_{MgAlO_{2.5}}^{Brg})^2$ (detailed can be found in Supplementary text and Table S2). Abbreviations: Brg, bridgmanite; CF: calcium ferrite-type structure of MgAl₂O₄; Per, periclase; OV: MgAlO_{2.5}; CC: AlAlO₃. Red symbols and lines represent the OV component and its variation with temperature, respectively, while these blue ones represent those for the CC component.

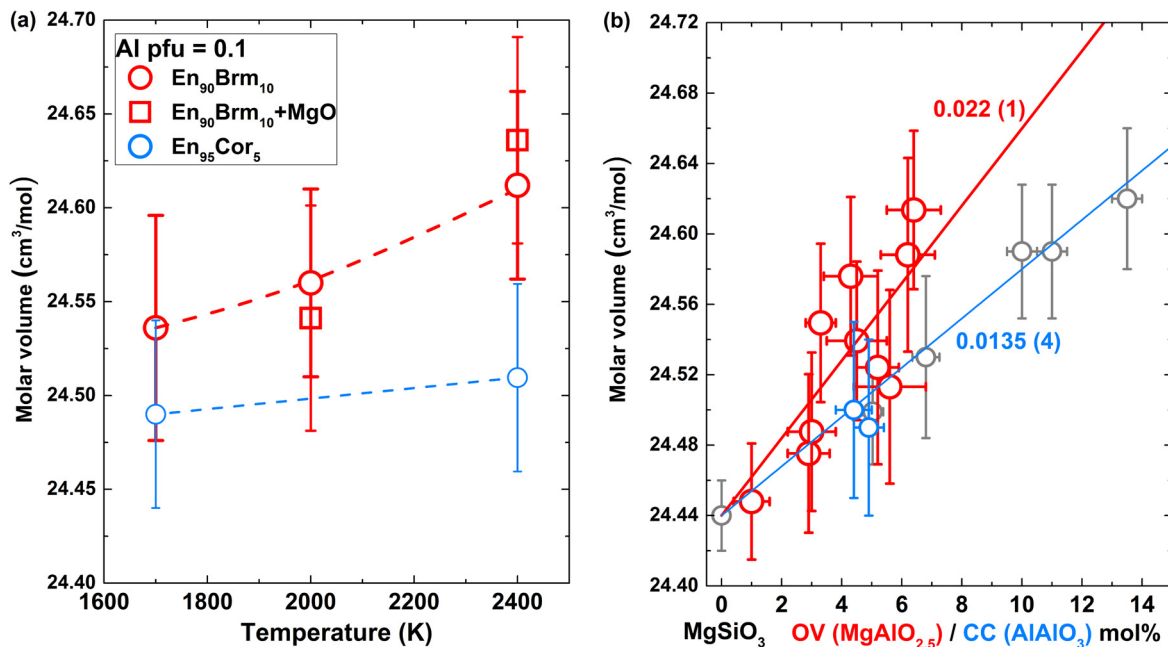
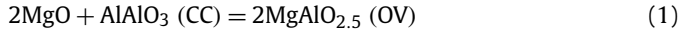


Fig. 4. Molar volume of bridgmanite (a) with an Al pfu of 0.1 as a function of temperature and (b) CC (AlAlO₃, blue circles) or OV (MgAlO_{2.5}, red circles) in mol%. The number is the linear increase rate for molar volume with CC and OV component and that in parentheses represents the standard deviation of the last digit. Black symbols are data from Liu et al. (2017b). Dashed lines in (a) are the tendency of the data with temperature, while solid lines are linear fitting results.

4. Discussion

4.1. Inverse correlations between OV and CC contents in bridgmanite

To interpret the inversely correlated variation of OV and CC contents with temperature in bridgmanite synthesized from $\text{En}_{90}\text{Brm}_{10}$, the variation of these two components can be expressed by the following reaction:



Because some amount of the CC component is present in what should have been MgO-free samples of $\text{En}_{90}\text{Brm}_{10}$ at 1700 and 2000 K, there may also have been small amounts of periclase in these samples according to reaction (1). However, we did not find any periclase by XRD or BSE observations. It is possible that the amount of periclase may be too low to be detected by XRD, and that tiny periclase grains may have been polished out from the surface prior by SEM analysis. The Gibbs free energy of reaction of (1) can be written as:

$$2\mu_{\text{MgO}}^{\text{Pc}} + \mu_{\text{AlAlO}_3}^{\text{Brg}} = 2\mu_{\text{MgAlO}_{2.5}}^{\text{Brg}} \quad (2)$$

where $\mu_{\text{MgO}}^{\text{Pc}}$, $\mu_{\text{Al}_2\text{O}_3}^{\text{Brg}}$, and $\mu_{\text{MgAlO}_{2.5}}^{\text{Brg}}$ are the chemical potentials of MgO in periclase and AlAlO_3 and $\text{MgAlO}_{2.5}$ components in bridgmanite, respectively. We use the non-ideal solution model of the chemical compositions in bridgmanite. The chemical potentials in these components can be written as:

$$\mu_{\text{MgO}}^{\text{Pc}} = \mu_{\text{MgO}}^{\circ\text{Pc}} + RT \ln a_{\text{MgO}}^{\text{Pc}} \quad (3)$$

$$\mu_{\text{AlAlO}_3}^{\text{Brg}} = \mu_{\text{AlAlO}_3}^{\circ\text{Brg}} + RT \ln a_{\text{AlAlO}_3}^{\text{Brg}} \quad (4)$$

$$\mu_{\text{MgAlO}_{2.5}}^{\text{Brg}} = \mu_{\text{MgAlO}_{2.5}}^{\circ\text{Brg}} + RT \ln a_{\text{MgAlO}_{2.5}}^{\text{Brg}} \quad (5)$$

where $\mu_{\text{MgO}}^{\circ\text{Pc}}$, $\mu_{\text{AlAlO}_3}^{\circ\text{Brg}}$, and $\mu_{\text{MgAlO}_{2.5}}^{\circ\text{Brg}}$ are the chemical potentials of the (hypothetical) endmembers of these three components, and $a_{\text{MgO}}^{\text{Pc}}$, $a_{\text{AlAlO}_3}^{\text{Brg}}$, and $a_{\text{MgAlO}_{2.5}}^{\text{Brg}}$ are their activities. By substituting Eqs. (3), (4), and (5) into Eq. (2), the standard state Gibbs free energy change of reaction (1) can be then expressed as:

$$\Delta G_{R1}^0 = 2\mu_{\text{MgAlO}_{2.5}}^{\circ\text{Brg}} - 2\mu_{\text{MgO}}^{\circ\text{Pc}} - \mu_{\text{AlAlO}_3}^{\circ\text{Brg}} = 2RT \ln a_{\text{MgO}}^{\text{Pc}} + RT \ln a_{\text{AlAlO}_3}^{\text{Brg}} - 2RT \ln a_{\text{MgAlO}_{2.5}}^{\text{Brg}} \quad (6)$$

Based on the symmetric regular solution model (Thompson, 1967), the activities of AlAlO_3 and $\text{MgAlO}_{2.5}$ component in bridgmanite can be expressed as:

$$\begin{aligned} RT \ln a_{\text{AlAlO}_3}^{\text{Brg}} &= RT \ln (X_{\text{Al}_2\text{O}_3}^{\text{Brg}} \cdot \gamma_{\text{AlAlO}_3}^{\text{Brg}}) \\ &= RT \ln X_{\text{AlAlO}_3}^{\text{Brg}} + W_{\text{AlAlO}_3}^{\text{Brg}} (1 - X_{\text{AlAlO}_3}^{\text{Brg}})^2 \end{aligned} \quad (7)$$

$$\begin{aligned} RT \ln a_{\text{MgAlO}_{2.5}}^{\text{Brg}} &= RT \ln (X_{\text{MgAlO}_{2.5}}^{\text{Brg}} \cdot \gamma_{\text{MgAlO}_{2.5}}^{\text{Brg}}) \\ &= RT \ln X_{\text{MgAlO}_{2.5}}^{\text{Brg}} + W_{\text{MgAlO}_{2.5}}^{\text{Brg}} (1 - X_{\text{MgAlO}_{2.5}}^{\text{Brg}})^2 \end{aligned} \quad (8)$$

where $X_{\text{MgAlO}_{2.5}}^{\text{Brg}}$ and $X_{\text{AlAlO}_3}^{\text{Brg}}$, respectively, are the mole fraction of the $\text{MgAlO}_{2.5}$ and AlAlO_3 components in the bridgmanite; $\gamma_{\text{MgAlO}_{2.5}}^{\text{Brg}}$ and $\gamma_{\text{AlAlO}_3}^{\text{Brg}}$ are an effective coefficient for expressing the non-ideality of mixing; $W_{\text{AlAlO}_3}^{\text{Brg}}$ and $W_{\text{MgAlO}_{2.5}}^{\text{Brg}}$ are interaction parameters for the degree of the non-ideality of mixing. For reaction (1), from Raoult's law (Guggenheim, 1937), we assume the activity of the MgO component in periclase as its mole fraction ($a_{\text{MgO}}^{\text{Pc}} = X_{\text{MgO}}^{\text{Pc}}$). The Gibbs free energy change of reaction (1) can then be expressed as:

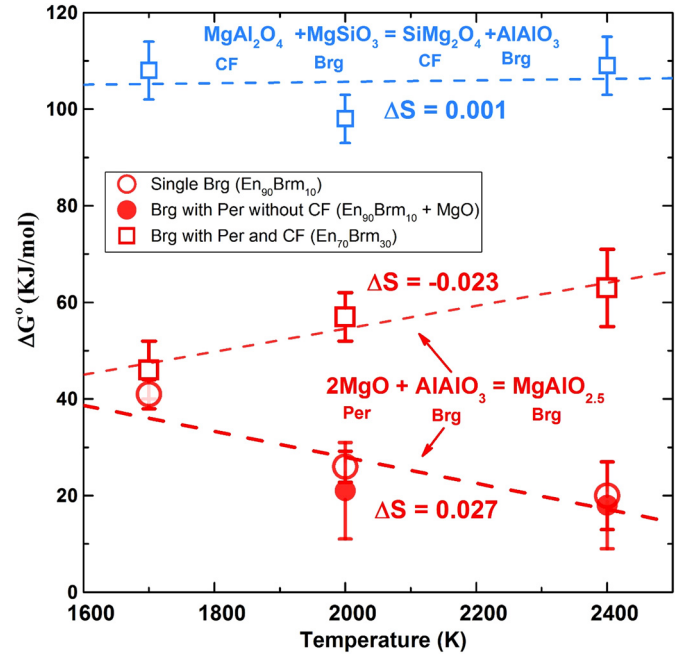


Fig. 5. Gibbs free energy of reaction (1) for single-phase bridgmanite for $\text{En}_{90}\text{Brm}_{10}$ (red open circles), bridgmanite coexisting with periclase for mixture of $\text{En}_{90}\text{Brm}_{10}$ and MgO (red solid circles) and bridgmanite with periclase and CF-phase from $\text{En}_{70}\text{Brm}_{30}$ (red squares), and that of reaction (12) for bridgmanite coexisting with periclase and CF phase for $\text{En}_{70}\text{Brm}_{30}$ (blue squares). Dashed lines are the linear fitting results ($\Delta G = \Delta H - T\Delta S$) and the slope is ΔS . Abbreviations: Brg, bridgmanite; CF: calcium ferrite-type structure of MgAl_2O_4 ; Per, periclase.

$$\begin{aligned} \Delta G_{R1}^0 &= -RT \ln \frac{(X_{\text{MgAlO}_{2.5}}^{\text{Brg}})^2}{(X_{\text{MgO}}^{\text{Pc}})^2 X_{\text{AlAlO}_3}^{\text{Brg}}} + W_{\text{AlAlO}_3}^{\text{Brg}} (1 - X_{\text{AlAlO}_3}^{\text{Brg}})^2 \\ &\quad - 2W_{\text{MgAlO}_{2.5}}^{\text{Brg}} (1 - X_{\text{MgAlO}_{2.5}}^{\text{Brg}})^2 \end{aligned} \quad (9)$$

Here we estimate W_1 and W_2 by an empirical method for the non-ideality of solid solutions due to a mismatch of the component volumes using the following formula (Davies and Navrotsky, 1983; Akaogi and Ito, 1999):

$$W_G = 100.8 \cdot \Delta V - 0.4 \text{ kJ/mol} \quad (10)$$

$$\Delta V = \frac{V_A - V_B}{(V_A + V_B)/2} \quad (11)$$

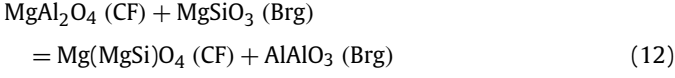
where V_A and V_B are the molar volumes of the larger and smaller components, respectively. We then obtain $W_{\text{AlAlO}_3}^{\text{Brg}}$ and $W_{\text{MgAlO}_{2.5}}^{\text{Brg}}$ values of 5.0 ± 0.2 and 8.0 ± 0.8 KJ/mol from the present molar volume results. As shown in Fig. 5, the derived ΔG_{R1}^0 would decrease from 41 ± 8 KJ/mol at 1700 K to 26 ± 6 KJ/mol at 2000 K to 20 ± 10 KJ/mol at 2400 K for the reaction of $\text{En}_{90}\text{Brm}_{10}$. ΔG_{R1}^0 for the mixture of $\text{En}_{90}\text{Brm}_{10} + \text{MgO}$ at 2000 (21 ± 10 KJ/mol) and 2400 K (18 ± 9 KJ/mol) are consistent with those without MgO within uncertainties. By fitting the present experimental data in the absence of a CF-phase to a linear function of $\Delta G_{R1}^0 = \Delta H_{R1}^0 - T\Delta S_{R1}^0$, we obtained $\Delta S_{R1}^0 = -(\frac{\partial \Delta G_{R1}^0}{\partial T})_P = 27 \pm 9$ J/mol·K. This result suggests that high temperatures promote the forward progression of this reaction and thereby increase the OV content by consuming the CC component and periclase.

4.2. Al partitioning in bridgmanite, periclase, and the CF-phase

The appearing periclase in addition to bridgmanite in the $\text{En}_{70}\text{Brm}_{30}$ sample can also be explained by the Eqs. (1)–(9), although periclase contains only a very trace amount of Al_2O_3 . By

using the compositions of bridgmanite from En₇₀Brm₃₀ and assuming the periclase contains pure MgO, we obtained the ΔG_{R1}^0 values of 47 ± 7 , 57 ± 5 , and 63 ± 8 kJ·mol⁻¹ at 1700, 2000, and 2400 K, respectively. The derived ΔS_{R1}^0 is -23 ± 7 J/mol·K, suggesting that the CC component is more favored at high temperature compared with the OV component in bridgmanite for the En₇₀Brm₃₀ sample (Fig. 3b).

The exchange of Al³⁺ between bridgmanite and the CF-phase is expressed by the reaction:



This reaction (12) represents the exchange of Al and Si between the CF-phase and bridgmanite, and so the OV component is not included. Mg²⁺ and Si⁴⁺ in the CF-phase would substitute for two Al³⁺ in octahedral sites through a charge-coupled substitution, although the Mg(MgSi)O₄ (i.e., Mg₂SiO₄) endmember CF-phase cannot exist in the lower mantle because it is less stable than the mixture of MgSiO₃ bridgmanite and MgO periclase (Kojitani et al., 2007b). The Gibbs free energy change for reaction (12) can be expressed as:

$$\Delta G_{R12}^0 = RT \ln a_{\text{MgSiO}_3}^{\text{Brg}} + RT a_{\text{MgAl}_2\text{O}_4}^{\text{CF}} - RT \ln a_{\text{AlAlO}_3}^{\text{Brg}} \\ - RT \ln a_{\text{Mg(MgSi)O}_4}^{\text{CF}} \quad (13)$$

Reaction (12) can be regarded as two binary systems of MgSiO₃–Al₂O₃ and MgAl₂O₄–Mg(MgSi)O₄. The activity coefficients for those components in bridgmanite and CF-phase can be expressed as:

$$a_{\text{AlAlO}_3}^{\text{Brg}} = (X_{\text{AlAlO}_3}^{\text{Brg}} \cdot \gamma_{\text{AlAlO}_3}^{\text{Brg}})^2 \quad (14)$$

$$a_{\text{MgSiO}_3}^{\text{Brg}} = (\gamma_{\text{MgSiO}_3}^{\text{Brg}} \cdot \gamma_{\text{MgSiO}_3}^{\text{Brg}})^2 \quad (15)$$

$$a_{\text{MgAl}_2\text{O}_4}^{\text{CF}} = (X_{\text{MgAl}_2\text{O}_4}^{\text{CF}} \cdot \gamma_{\text{MgAl}_2\text{O}_4}^{\text{CF}})^2 \quad (16)$$

$$a_{\text{Mg(MgSi)O}_4}^{\text{CF}} = (X_{\text{SiMg}_2\text{O}_4}^{\text{CF}} \cdot \gamma_{\text{Mg(MgSi)O}_4}^{\text{CF}})^2 \quad (17)$$

The activity coefficients can be written as:

$$RT \ln \gamma_{\text{AlAlO}_3}^{\text{Brg}} = W_{\text{Al}}^{\text{Brg}} (1 - X_{\text{AlAlO}_3}^{\text{Brg}})^2 \quad (18)$$

$$RT \ln \gamma_{\text{MgSiO}_3}^{\text{Brg}} = W_{\text{Al}}^{\text{Brg}} (1 - X_{\text{MgSiO}_3}^{\text{Brg}})^2 \quad (19)$$

$$RT \ln \gamma_{\text{Mg(MgSi)O}_4}^{\text{CF}} = W_{\text{SiAl}}^{\text{CF}} (1 - X_{\text{Mg(MgSi)O}_4}^{\text{CF}})^2 \quad (20)$$

$$RT \ln \gamma_{\text{MgAl}_2\text{O}_4}^{\text{CF}} = W_{\text{SiAl}}^{\text{CF}} (1 - X_{\text{MgAl}_2\text{O}_4}^{\text{CF}})^2 \quad (21)$$

where $X_{\text{MgAl}_2\text{O}_4}^{\text{CF}}$ and $X_{\text{Mg(MgSi)O}_4}^{\text{CF}}$ are the mole fractions of MgAl₂O₄ and Mg(MgSi)O₄ in the CF-phase, respectively. ΔG_{R12}^0 can be expressed as:

$$\Delta G_{R12}^0 = -2RT \ln \frac{X_{\text{Mg(MgSi)O}_4}^{\text{CF}} X_{\text{AlAlO}_3}^{\text{Brg}}}{X_{\text{MgAl}_2\text{O}_4}^{\text{CF}} X_{\text{MgSiO}_3}^{\text{Brg}}} + 2W_{\text{SiAl}}^{\text{CF}} (1 - 2X_{\text{MgAl}_2\text{O}_4}^{\text{CF}}) \\ + 2W_{\text{Al}}^{\text{Brg}} (2X_{\text{AlAlO}_3}^{\text{Brg}} - 1) \quad (22)$$

We used Eqs. (10) and (11) to fit the molar volume data for the CF-phase obtained by Kojitani et al. (2007b), yielding $W_{\text{SiAl}}^{\text{CF}}$ of 0.6 kJ·mol⁻¹. The derived ΔC_{R12}^0 changes from 108 ± 6 kJ·mol⁻¹ at 1700 K to 98 ± 5 kJ·mol⁻¹ at 2000 K and to 109 ± 6 kJ·mol⁻¹ at 2400 K. Because these changes are identical within experimental error, ΔS_{R12}^0 is essentially zero within analytical uncertainties (1 ± 16 J/mol·K, Fig. 5). Thus, reaction (12) will proceed in the forward direction because of the entropy of mixing. As such, both

Al₂O₃ and Mg₂SiO₄ should be present only as minor impurities in the bridgmanite and CF-phase, respectively, although their concentrations will increase with temperature.

Both experimental and thermodynamics results indicate that high temperatures promote the reaction of CC-bearing bridgmanite with coexisting periclase to form OV-rich bridgmanite and the total Al-content of bridgmanite coexisting with only periclase is nearly constant for En₉₀Brm₁₀ with and without MgO sample (Fig. 3a). In contrast, for bridgmanite with CF-phase and periclase, the addition of an external Al-reservoir in the form of a CF-phase induces a total Al increase with temperature (Fig. 3b). This increase Al at high temperature would favor the CC content and the OV content thus slightly increase or keep almost constant, which shows that the OV/CC molar ratio remains almost constant at 0.5–0.6 in the 1700–2400 K range. In summary, the OV component content increases with temperature, especially for bridgmanite coexistence with periclase without a CF-phase. An increase of the OV content with temperature is therefore expected to occur in peridotitic or pyrolytic bulk compositions (bridgmanite coexisting with periclase) rather than basaltic compositions (bridgmanite coexisting with stishovite and a CF-phase).

5. Implications

5.1. Effect of the OV and CC component with temperatures on the elasticity of bridgmanite

An increase in the OV content with temperature should cause a decrease in bulk modulus because of its low density at high temperature because that a looser structure should have a capability to be more substantially compressed (Brodholt, 2000). The isothermal bulk modulus of aluminous bridgmanite has been thoroughly investigated and the various reported values of aluminous bridgmanite with a pyrolytic Al composition (Al pfu = 0.1) range from 232 to 272 GPa (e.g., Zhang and Weidner, 1999; Daniel et al., 2001; Walter et al., 2004, 2006; Andrault et al., 2001, 2007). This large variation in bulk moduli could be related to variable OV contents in bridgmanite in response to different temperature and/or pressure conditions. In addition to the temperature effect demonstrated in the present study, increasing pressure has been shown to largely decrease the OV content (Liu et al., 2017a). Andrault et al. (2007) demonstrated that aluminous bridgmanite synthesized at 2300 K has a significantly lower bulk modulus (244 GPa) compared with that at lower temperature of 1800 K (272 GPa), and that the bulk modulus of bridgmanite synthesized at high pressures of 47–56 GPa (272 GPa) is substantially higher than that at lower pressures of 23–37 GPa (236 GPa). The increase of the OV content with increasing temperature and decreasing pressure and possible low bulk modulus of the OV component could explain these results. It is apparent that varying the temperature and pressure during synthesis can significantly affect the defect chemistry and thereby elastic properties of bridgmanite. The differences of bulk moduli between 272 and 244 GPa and 272 and 236 GPa potentially causes variations in bulk sound velocity of 5 to 7%, which are extremely large from a seismological point of view.

Although elasticity studies of aluminous bridgmanite, especially OV-bearing bridgmanite, are scarce, we simply argue here that the elasticity of aluminous bridgmanite based on Birch's law (Birch, 1952), namely, the linear relationships between compressional wave velocity (V_P) and density. We also assume a linear relationship between shear wave velocity (V_S) and density. Jackson et al. (2004) reported $V_P = 10.84$ km/s and $V_S = 6.47$ km/s for polycrystalline MgSiO₃ bridgmanite and $V_P = 10.75$ km/s and $V_S = 6.35$ km/s for Mg_{0.95}Al_{0.1}Si_{0.95}O₃ bridgmanite under ambient conditions. As Jackson et al. (2004) argued, the shear modu-

lus, G , decreases significantly by 4% for 5 mol% Al_2O_3 component, while the adiabatic bulk modulus, K_S , is not affected. As a result, V_S decreases substantially (−1.8%), whereas V_P decreases only slightly (−0.8%). The present study shows that the density of $\text{Mg}_{0.95}\text{Al}_{0.1}\text{Si}_{0.95}\text{O}_3$ bridgmanite is 4.101 g/cm^3 under ambient conditions, which is slightly higher by 0.8% than that obtained by Jackson et al. (2004) (4.081 g/cm^3). This leads to an increase of V_P and V_S to 10.82 and 6.49 km/s, respectively. In the present study, the OV-dominated bridgmanite with the same amount of Al_2O_3 , namely, $\text{MgAl}_{0.1}\text{Si}_{0.9}\text{O}_{2.95}$ should have a density of 4.035 g/cm^3 , which is significantly lower by 1.9% than that of the CC component (4.112 g/cm^3). This leads to large velocity drops, namely, $V_P = 10.58$ and $V_S = 6.02$ km/s. This evaluation suggests that the OV component decreases velocities 14 times more strongly than the CC component compared with the MgSiO_3 bridgmanite end-member.

In a pyrolite composition, all Al would be contained in bridgmanite and a CF-phase is thus absent. In this case, the CC and OV components, respectively, decrease and increase from 3.5 to 1.6 mol% and from 3.0 to 6.4 mol% with increasing temperature from 1700 to 2400 K, as shown in the present study. These values suggest that the V_P and V_S of bridgmanite in a pyrolitic mantle decrease by −0.7% and −2.5% with increasing temperature from 1700 to 2400 K purely due to a change in the Al substitution mechanism. Aizawa et al. (2004) reported the temperature dependence of the adiabatic bulk and shear moduli are −0.029 and −0.024 GPa/K, respectively. Katsura et al. (2010) suggested that thermal expansion of bridgmanite at the top of the lower mantle is 2×10^{-5} K. These data suggest that V_P and V_S of bridgmanite decrease with increasing temperature from 1700 to 2400 K by −2.5% and −2.7%, respectively, because of anharmonic effects. The change in Al substitution mechanisms thus enhances V_P and V_S reduction with elevating temperature by 3% and 5% in comparison with the anharmonic effects.

5.2. Volatile storage in the warm ambient lower mantle and cold subducted slabs

The presence of OV in bridgmanite may provide storage sites to incorporate hydroxyl (Navrotsky, 1999; Murakami et al., 2002) and noble gases with suitable atomic radii such as argon (1.64 Å), neon (1.18 Å), and helium (0.90 Å) (Shcheka and Keppler, 2012), although hydroxyl storage in the lower mantle is still under debate (e.g., Murakami et al., 2002; Litasov et al., 2003; Bolfan-Casanova et al., 2003). In a pyrolitic composition, bridgmanite contains as much as 5 mol% OV component at 27 GPa and 2000 K, which is enough to explain a maximum of 1 wt.% water and argon incorporated in bridgmanite in the uppermost part of the lower mantle (Murakami et al., 2002; Litasov et al., 2003; Shcheka and Keppler, 2012), although this component will rapidly decrease with increasing depth (Liu et al., 2017a). The present results show that the OV content decreases with decreasing temperature (0.5 mol% per 100 K), and the volatile storage capacity should therefore decrease to almost zero in subducted slabs because their typical temperature is significantly lower by ~800 K than the warm ambient lower mantle (Eberle et al., 2002).

It is also important to consider that pyrolitic bridgmanite contains significant amounts of iron (Fe) in addition to Al, and that the oxidation of Fe would prefer to form the charge-coupled FeAlO_3 component (Frost and Langenhorst, 2002). This fact may even decrease the OV component in bridgmanite in the ambient lower mantle. Here, we consider Mg^{2+} , Fe^{2+} , Fe^{3+} , and Al^{3+} as the major cations in pyrolitic bridgmanite and found that bridgmanite will contain about 3 ± 1 mol% OV and 6 ± 1 mol% CC (FeAlO_3 plus AlAlO_3) at 26 GPa and 1900–2000 K by assuming a Fe^{3+} fraction to the total iron ($\text{Fe}^{3+}/\Sigma\text{Fe}$) of 60% in a reduced lower mantle

(McCammon, 1997; Frost et al., 2004) and Fe^{3+} preferably substituting into the Mg^{2+} site in the uppermost lower mantle (Fujino et al., 2012). This small amount of OV component will thus typically decrease to zero in cold subducted slabs because of a very low temperature. To fully understand the volatile cycle in the lower mantle, further studies is required to clarify the concentration of trivalent cation such as Fe^{3+} and Al^{3+} , the coexisting phases such as periclase in the pyrolite mantle model and stishovite in the MORB model, and the redox environment on the chemistry defects of bridgmanite.

5.3. Explanation of mantle plumes and slab stagnation in the lower mantle

The rheological properties of bridgmanite are expected to control lower-mantle dynamics due to its dominant abundance. Karato and Wu (1993) suggested that diffusion creep should dominate bridgmanite creep. The OV component will increase atomic diffusivity in bridgmanite because of oxygen vacancy and therefore soften the lower mantle. Recent seismic tomography showed that mantle plumes are straight and vertical in the lower mantle, but bend significantly in the upper mantle (French and Romanowicz, 2015). This implies that bridgmanite is more effectively softened at high temperature than upper mantle minerals. Nevertheless, the activation enthalpy of olivine dislocation creep is about 500 kJ/mol (e.g., Karato and Jung, 2003), whereas that of Si diffusion in bridgmanite is smaller, about 300 kJ/mol (Yamazaki et al., 2000; Dobson et al., 2008; Xu et al., 2011), which is against the expectation from the shapes of plumes. However, since the vacancy concentration in bridgmanite will increase with temperature, diffusion creep should be more enhanced than expected from the activation enthalpy of Si diffusion because of the OV component. Our conclusion of the present study, namely the positive temperature dependence of the OV content, may therefore explain seismic observations regarding mantle plumes.

Fukao and Obayashi (2013) depicted slab stagnation in the mid-mantle down to 1000-km depth. Similar to the discussion above, a nearly absent OV component should lead to much stiffer subducted slabs than the ambient mantle down to 1000 km because of the low temperature, which facilitates slab penetration into the lower mantle. However, the OV content in the ambient mantle also becomes nearly zero in deeper regions because of the negative pressure dependence of the OV content. The loss of viscosity contrast should impede slab subduction into the deep lower mantle and lead to slab stagnation in the mid-mantle. Our study thus provides an additional explanation for the seismically-observed slab stagnation in the mid-mantle.

6. Conclusions

We have clarified the temperature dependence of the OV content of bridgmanite in the presence of periclase without or with a CF-phase. In bridgmanite without a CF-phase, the OV content significantly increases with temperature by consuming the CC component and periclase as a result of the constant Al content. In bridgmanite coexisting with a CF-phase and periclase, the OV increase largely relative to the OV components with temperature by the supply of Al from the CF-phase. The formation of the OV component from the CC component and periclase is favored at high temperature, whereas the supply of Al from the CF-phase to bridgmanite is due to the entropy of mixing. The present results can explain the lower bulk modulus of bridgmanite synthesized at higher temperatures and lower pressures, which results from the high proportion of an OV component. The derived molar volume of the OV bridgmanite endmember is 26.64

cm^3/mol , which is 4% higher than that of CC-endmember bridgmanite ($25.79 \text{ cm}^3/\text{mol}$) at ambient conditions. The OV component may thus cause lower velocities than the CC component at constant Al content in bridgmanite. Bridgmanite in the uppermost of the ambient lower mantle could contain significant amounts of volatiles such as noble gases and water. The storage capacity of volatiles in bridgmanite in subducted slabs should be significantly lower than that in the surrounding ambient mantle because of the lower slab temperatures. A decrease of OV component with decreasing temperature can cause an increase in the viscosity of bridgmanite from the warm ambient lower mantle to the surrounding cold subducted slabs. This fact may explain seismically observed slab stagnation and vertically straight plumes in the lower mantle. The present study helps to elucidate the complex chemistry of bridgmanite and is therefore important for understanding the geophysics and geochemistry of the Earth's lower mantle.

Acknowledgements

The authors thank D. Krauße for his technical assistance in electron microprobe analysis, and E.S. Posner, H. Fischer and S. Übelhack for their assistance with high-pressure assembly preparation. We also thank D.J. Frost for his discussion. The manuscript is greatly improved by the constructive comments by R.G. Trønnes and an anonymous reviewer and the editorial handling by J.P. Brodholt. Z.L. was financially supported by the Bayerisches Geoinstitut Visitor's Program. This study is also supported by research grants to T.K. (BMBF: 05K13WC2, 05K16WC2; DRC: 78527; DFG: KA3434/3-1, KA3434/7-1, KA3434/8-1, KA3434/9-1, KA3434/3-2, KA3434-11/1, KA3434-12/1).

Appendix A. Supplementary material

Supplementary material related to this article can be found online at <https://doi.org/10.1016/j.epsl.2018.10.014>.

References

- Aizawa, Y., Yoneda, A., Katsura, T., Ito, E., Saito, T., Suzuki, I., 2004. Temperature derivatives of elastic moduli of MgSiO_3 perovskite. *Geophys. Res. Lett.* 31 (1).
- Akaogi, M., Ito, E., 1999. Calorimetric study on majorite-perovskite transition in the system $\text{Mg}_4\text{Si}_4\text{O}_{12}\text{-Mg}_3\text{Al}_2\text{Si}_3\text{O}_{12}$: transition boundaries with positive pressure-temperature slope. *Phys. Earth Planet. Inter.* 114, 129–140.
- Andraut, D., Bolfan-Casanova, N., Guignot, N., 2001. Equation of state of lower mantle (Al,Fe)- MgSiO_3 perovskite. *Earth Planet. Sci. Lett.* 193, 501–508.
- Andraut, D., Bolfan-Casanova, N., Bouhifd, M.A., Guignot, N., Kawamoto, T., 2007. The role of Al-defects on the equation of state of Al-(Mg, Fe) SiO_3 perovskite. *Earth Planet. Sci. Lett.* 263, 167–179.
- Birch, F., 1952. Elasticity and constitution of the Earth's interior. *J. Geophys. Res.* 57, 227–286.
- Bolfan-Casanova, N., Keppler, H., Rubie, D.C., 2003. Water partitioning at 660 km depth and evidence for very low water solubility in magnesium silicate perovskite. *Geophys. Res. Lett.* 30, 1905.
- Brodholt, J.P., 2000. Pressure-induced changes in the compression mechanism of aluminous perovskite in the Earth's mantle. *Nature* 407, 620–622.
- Brown, J.M., Shankland, T.J., 1981. Thermodynamic parameters in the Earth as determined from seismic profiles. *Geophys. J. R. Astron. Soc.* 66, 579–596.
- Daniel, I.H., Cardon, H., Fiquet, G., Guyot, F., Mezouar, M., 2001. Equation of state of Al-bearing perovskite to lower mantle conditions. *Geophys. Res. Lett.* 28, 3789–3792.
- Davies, P.K., Navrotsky, A., 1983. Quantitative correlations of deviations from ideality in binary and pseudo-binary solid solutions. *J. Solid State Chem.* 46, 1–22.
- Dobson, D.P., Dohmen, R., Weidenbeck, M., 2008. Self-diffusion of oxygen and silicon in MgSiO_3 . *Earth Planet. Sci. Lett.* 270, 125–129.
- Eberle, M.A., Grasset, O., Sotin, C., 2002. A numerical study of the interaction between the mantle wedge, subducting slab, and overriding plate. *Phys. Earth Planet. Inter.* 134, 191–202.
- French, S.W., Romanowicz, B., 2015. Broad plumes rooted at the base of the Earth's mantle beneath major hotspots. *Nature* 525 (7567), 95–99.
- Frost, D.J., Langenhorst, F., 2002. The effect of Al_2O_3 on Fe-Mg partitioning between magnesio-wüstite and magnesium silicate perovskite. *Earth Planet. Sci. Lett.* 199, 227–241.
- Frost, D.J., Liebske, C., Langenhorst, F., McCammon, C.A., Trønnes, R.G., Rubie, D.C., 2004. Experimental evidence for the existence of iron-rich metal in the Earth's lower mantle. *Nature* 428, 409–412.
- Fujino, K., et al., 2012. Spin transition of ferric iron in Al-bearing Mg-perovskite up to 200 GPa and its implication for the lower mantle. *Earth Planet. Sci. Lett.* 317–318, 407–412.
- Fukao, Y., Obayashi, M., 2013. Subducted slabs stagnant above, penetrating through, and trapped below the 660 km discontinuity. *J. Geophys. Res., Solid Earth* 118, 2013JB010466.
- Guggenheim, E.A., 1937. Theoretical basis of Raoult's Law. *Trans. Faraday Soc.* 33, 151–159.
- Hirsch, L.M., Shankland, T.J., 1991. Point defects in silicate perovskite. *Geophys. Res. Lett.* 18, 1305–1308.
- Horiuchi, H., Ito, E., Weidner, D.J., 1987. Perovskite-type MgSiO_3 : single-crystal X-ray diffraction study. *Am. Mineral.* 72, 357–360.
- Irfune, T., 1994. Absence of an aluminous phase in the upper part of the Earth's lower mantle. *Nature* 370 (6485), 131–133.
- Ishii, T., et al., 2016. Generation of pressure over 40 GPa using Kawai-type multi-anvil press with tungsten carbide anvils. *Rev. Sci. Instrum.* 87, 024501.
- Jackson, J., Zhang, M.J., Bass, J.D., 2004. Sound velocities and elasticity of aluminous MgSiO_3 perovskite: implications for aluminum heterogeneity in Earth's lower mantle. *Geophys. Res. Lett.* 31, L10614.
- Karato, S., Jung, H., 2003. Effects of pressure on high-temperature dislocation creep in olivine. *Philos. Mag.* 83, 401–414.
- Karato, S., Wu, P., 1993. Rheology of the upper mantle: a synthesis. *Science* 260, 771–778.
- Katsura, T., Yoneda, A., Yamazaki, D., et al., 2010. Adiabatic temperature profile in the mantle. *Phys. Earth Planet. Inter.* 183, 212–218.
- Kirby, S.H., Stein, S., Okal, E.A., Rubie, D.C., 1996. Metastable mantle phase transformations and deep earthquakes in subducting oceanic lithosphere. *Rev. Geophys.* 34 (2), 261–306.
- Kojitani, H., Katsura, T., Akaogi, M., 2007a. Aluminum substitution mechanisms in perovskite-type MgSiO_3 : an investigation by Rietveld analysis. *Phys. Chem. Miner.* 34, 257–267.
- Kojitani, H., Hisatomi, R., Akaogi, M., 2007b. High-pressure phase relations and crystal chemistry of calcium ferrite-type solid solutions in the system $\text{MgAl}_2\text{O}_4\text{-Mg}_2\text{SiO}_4$. *Am. Mineral.* 92, 1112–1118.
- Litasov, K., Ohtani, E., Langenhorst, F., Yurimoto, H., Kubo, T., Kondo, T., 2003. Water solubility in Mg-perovskites and water storage capacity in the lower mantle. *Earth Planet. Sci. Lett.* 211 (1), 189–203.
- Liu, Z.D., Irfune, T., Nishi, M., Tange, Y., Arimoto, T., Shinmei, T., 2016. Phase relations in the system $\text{MgSiO}_3\text{-Al}_2\text{O}_3$ up to 52 GPa and 2000 K. *Phys. Earth Planet. Inter.* 257, 18–27.
- Liu, Z.D., Ishii, T., Katsura, T., 2017a. Rapid decrease of $\text{MgAlO}_{2.5}$ component in bridgmanite with pressure. *Geochem. Perspect. Lett.* 5, 12–18.
- Liu, Z.D., Nishi, M., Ishii, T., Fei, H.Z., Miyajima, N., Boffa Ballaran, T., Ohfuji, H., Sakai, T., Wang, L., Shcheka, S., Arimoto, T., Tange, Y., Higo, Y., Irfune, T., Katsura, T., 2017b. Phase relations in the system $\text{MgSiO}_3\text{-Al}_2\text{O}_3$ up to 2300 K at lower-mantle pressures. *J. Geophys. Res.* 10, 7775–7788.
- McCammon, C.A., 1997. Perovskite as a possible sink for ferric iron in the lower mantle. *Nature* 387, 694–696.
- Murakami, M., Hirose, K., Yurimoto, H., Nakashima, S., Takafuji, N., 2002. Water in Earth's lower mantle. *Science* 295, 1885–1887.
- Navrotsky, A., 1999. A lesson from ceramics. *Science* 284, 1788–1789.
- Navrotsky, A., et al., 2003. Aluminum in magnesium silicate perovskite: formation, structure, and energetics of magnesium-rich defect solid solutions. *J. Geophys. Res.* 108 (7), 2330.
- Shcheka, S.S., Keppler, H., 2012. The origin of the terrestrial noble-gas signature. *Nature* 490, 531–534.
- Stebbins, J.F., Kojitani, H., Akaogi, M., Navrotsky, A., 2003. Aluminum substitution in MgSiO_3 perovskite: investigation of multiple mechanisms by ^{27}Al NMR. *Am. Mineral.* 88, 1161–1164.
- Thompson, J.B., 1967. Thermodynamic properties of simple solutions. In: Abelson, P.H. (Ed.), *Research in Geochemistry*, vol. 2. Wiley, New York, pp. 340–361.
- Walter, M., Kubo, A., Yoshino, T., Brodholt, J., Koga, K.T., Ohishi, Y., 2004. Phase relations and equation-of-state of aluminous Mg-silicate perovskite and implications for Earth's lower mantle. *Earth Planet. Sci. Lett.* 222, 501–516.
- Walter, M., Trønnes, R.G., Armstrong, L.S., Lord, O., Caldwell, W.A., Clark, A.M., 2006. Subsolidus phase relations and perovskite compressibility in the system $\text{MgO-AlO}_{1.5}\text{-SiO}_2$ with implications for Earth's lower mantle. *Earth Planet. Sci. Lett.* 248, 77–89.
- Xu, Y., McCammon, C.A., Poe, B.T., 1998. The effect of alumina on the electrical conductivity of silicate perovskite. *Science* 282, 922–924.
- Xu, J., Yamazaki, D., Katsura, T., Wu, X., Remmert, P., Yurimoto, H., Chakraborty, S., 2011. Silicon and magnesium diffusion in a single crystal of MgSiO_3 perovskite. *J. Geophys. Res.* 116, B12205.

- Yamazaki, D., Kato, T., Yurimoto, H., Ohtani, E., Toriumi, M., 2000. Silicon self-diffusion in MgSiO_3 perovskite at 25 GPa. *Phys. Earth Planet. Inter.* 119, 299–309.
- Yoshino, T., Kamada, S., Zhao, C., Ohtani, E., Hirao, N., 2016. Electrical conductivity model of Al-bearing bridgmanite with implications for the electrical structure of the Earth's lower mantle. *Earth Planet. Sci. Lett.* 434, 208–219.
- Zhang, J., Weidner, D.J., 1999. Thermal equation of state of aluminum-enriched silicate perovskite. *Science* 284, 782–784.